

Detection of Far Infrared Emission from Galaxies and Quasars in the Galactic Extinction Map by Stacking Analysis

Toshiya KASHIWAGI¹, Kazuhiro YAHATA^{1,2}, and Yasushi SUTO^{1,3,4}

¹*Department of Physics, The University of Tokyo, Tokyo 113-0033*

²*present address: Canon Inc. Ohta-ku, Tokyo 146-8501*

³*Research Center for the Early Universe, School of Science, The University of Tokyo, Tokyo 113-0033*

⁴*Department of Astrophysical Sciences, Princeton University, Princeton, NJ 08544, USA
kashiwagi@utap.phys.s.u-tokyo.ac.jp*

(Received 2012 July 29; accepted 2012 November 30)

Abstract

We have performed stacking image analyses of galaxies over the Galactic extinction map constructed by Schlegel, Finkbeiner & Davis (1998). We select $\sim 10^7$ galaxies in total from the Sloan Digital Sky Survey (SDSS) DR7 photometric catalog. We detect clear signatures of the enhancement of the extinction in r -band, ΔA_r , around galaxies, indicating that the extinction map is contaminated by their FIR (far infrared) emission. The average amplitude of the contamination per galaxy is well fitted to $\Delta A_r(m_r) = 0.64 \times 10^{0.17(18-m_r)}$ [mmag]. While this value is very small, it is directly associated with galaxies and may have a systematic effect on galaxy statistics. Indeed this correlated contamination leads to a relatively large anomaly of galaxy surface number densities against the SFD extinction A_{SFD} discovered by Yahata et al. (2007). We model the radial profiles of stacked galaxy images, and find that the FIR signal around each galaxy does not originate from the central galaxy alone, but is dominated by the contributions of nearby galaxies via galaxy angular clustering. The separation of the single galaxy and the clustering terms enables us to infer the statistical relation of the FIR and r -band fluxes of galaxies and also to probe the flux-weighted cross-correlation of galaxies, down to the magnitudes that are difficult to probe directly for individual objects. We repeat the same stacking analysis for SDSS DR6 photometric quasars and discovered the similar signatures but with weaker amplitudes. The implications of the present results for galaxy and quasar statistics and for correction to the Galactic extinction map are briefly discussed.

Key words: ISM: dust, extinction — cosmology: observations

1. Introduction

Galactic extinction is the most fundamental correction that should be applied to virtually all astronomical data. The most widely used map for the purpose is constructed by Schlegel, Finkbeiner & Davis (1998; hereafter, SFD). They first made dust temperature and emissivity maps (0.7 FWHM spatial resolution) from COBE/DIRBE data at $100 \mu\text{m}$ and $240 \mu\text{m}$. Then a finer resolution map was created for dust emission (6.1 FWHM angular resolution) from IRAS/ISSA data at $100 \mu\text{m}$ using the COBE temperature map as a calibrator. Finally they constructed the maps of reddening and extinction assuming a simple linear relation between far infrared (FIR) flux at $100 \mu\text{m}$ and dust column density with a temperature correction for dust emissivity. As is clear from their construction procedure, the SFD map *does not* correspond to absorption-weighted, as required for most purposed in astronomy, but is an emission-weighted dust extinction map.

This motivated Yahata et al. (2007; hereafter Y07) to examine the validity of the assumed proportionality between extinction and emissivity using the surface density of SDSS (York et al. 2000) galaxies in a given apparent magnitude range as a calibrator. Surprisingly, Y07 found that the galaxy surface densities *increase* against

the value of the extinction $A_{r,\text{SFD}}$ for low extinction regions ($A_{r,\text{SFD}} < 0.1$); see their Figure 4. After several careful analyses, they concluded that this anomaly originates from the far infrared (FIR) emission from the SDSS galaxies themselves. If such additional FIR emissions from extra-galactic objects are incorrectly interpreted as those from the Galactic dust, the extinction of those regions is overestimated. The amount of the FIR emission would be an increasing function of the surface number density of galaxies, and the correlation between them should be visible especially where the Galactic extinction is small. Moreover the correlation should become even stronger after correction using the contaminated extinction value.

Although the proposal of Y07 for the origin of the anomaly is reasonable, it is admittedly based on indirect and circumstantial evidence. In the present *paper*, we report on a detection of FIR emission signatures from SDSS galaxies and quasars through a stacking analysis of the SFD map. The amount of the FIR emission from those objects is statistically consistent with that required to explain the anomaly discovered by Y07.

The present paper is organized as follows; in §2 we describe part of the SDSS DR7 data catalog that we use in the analysis. After presenting the stacking analysis method, we show the stacked images and the resulting

fit to the analytical profile. Section 3 discusses the physical interpretation of the extracted parameters for FIR emission from SDSS galaxies and comparison with the cross-correlation with IRAS PSCz catalog. We also repeat the similar stacking analysis for SDSS DR6 photometric quasars in Section 4. Section 5 summarizes the conclusions. Finally in Appendix we show the IRAS Point Spread Function that we measure.

2. Stacking analysis

2.1. SDSS DR7 Data

In the following analysis, we use the SDSS DR7 photometric galaxy catalog, which covers 11663 deg² of sky area, with photometry in five passbands; u , g , r , i , and z (For more details of the photometric data, see Stoughton et al. 2002; Gunn et al. 1998; Gunn et al. 2006; Fukugita et al. 1996; Hogg et al. 2001; Ivezić et al. 2004; Smith et al. 2002; Tucker et al. 2006; Padmanabhan et al. 2008; Pier et al. 2003). According to photometry processing flags, we carefully remove bad photometry data and fast-moving objects, which are likely in the Solar system or associated with the interplanetary dust. We also exclude objects in masked regions to avoid unreliable photometry data. For more details of our data selection, see Yahata et al. (2007).

Our analysis below does not exclude the galaxies that are also detected by IRAS PSCz (Saunders et al. 2000; see §3) that are removed in the SFD map. We made sure that this has a negligibly small effect on our result because of the small number of overlapped galaxies.

2.2. Stacking Method

As discussed by Y07, the amount of FIR emission from SDSS galaxies that explains the anomaly is very small, and it is impossible to detect for individual galaxies. Therefore we stack those regions of the SFD map centered at the positions of SDSS photometric galaxies (in this section) or quasars (in appendix) over their appropriate magnitude bins. For that purpose, we use a contiguous region in the SDSS DR7 photometric catalog as shown in Figure 1.

The original SFD map divides all sky area into $2'37 \times 2'37$ pixels and the extinction value is provided for the central position of each pixel. The histograms of $A_{r,SFD}$ evaluated at those pixels as a function of the number of galaxies with $15.5 < m_r < 20.5$ within the pixel, $N_{g,pix}$, are shown in Figure 2. While the overall shapes of the histograms are very similar for different $N_{g,pix}$, the normalized probability density function (PDF) plotted in Figure 3 exhibits the small but systematic shift toward the larger $A_{r,SFD}$ with increasing $N_{g,pix}$. This indicates the correlation of the Galactic extinction and the background galaxies that will be extensively discussed in the present paper.

First we show the result of stacked SFD map images centered at photometric galaxies in the r -band magnitude range of $17.5 < m_r < 19.4$ randomly selected from a contiguous region in Figure 1. In this procedure we evaluate the value of $A_{r,SFD}$ on $0'2 \times 0'2$ pixels over $40' \times 40'$ images by cloud-in-cell interpolation of the 4 nearest neigh-

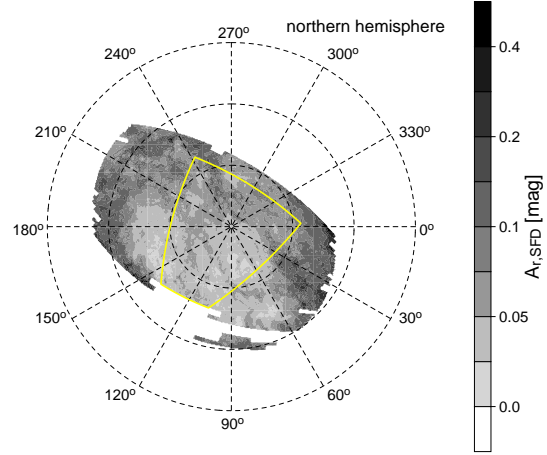


Fig. 1. The region of the sky used for the present analysis, which is shaded according to the extinction value $A_{r,SFD}$. The yellow lines indicate the inner regions used for comparison in Subsection 2.3.

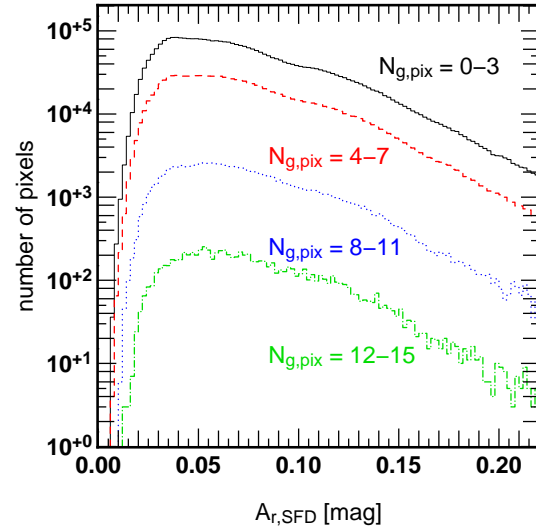


Fig. 2. Histograms of $A_{r,SFD}$ for $2'37 \times 2'37$ pixels over our selected survey region of SDSS DR7 as a function of the number of galaxies within the pixel, $N_{g,pix}$; $N_{g,pix} = 0-3$ in black, 4-7 in red, 8-11 in blue, and 12-15 in green.

bors in the original SFD pixels. Upper panels of Figure 4 clearly show the presence of the strong feature of $A_{r,SFD}$ around SDSS galaxies, which becomes more pronounced as increasing the number of stacked galaxies. For reference, lower panels of Figure 4 show the stacked SFD map images centered at the same number of randomly chosen positions from the same region of the corresponding top panels. This result directly confirms the interpretation of Y07 that the SFD map is contaminated by the FIR emission from SDSS galaxies.

2.3. Radial profiles of galaxies

To estimate the dependence of the contribution to $A_{r,SFD}$, or equivalently the amount of the FIR emission, on galaxy r -band magnitudes, we stack the images at the

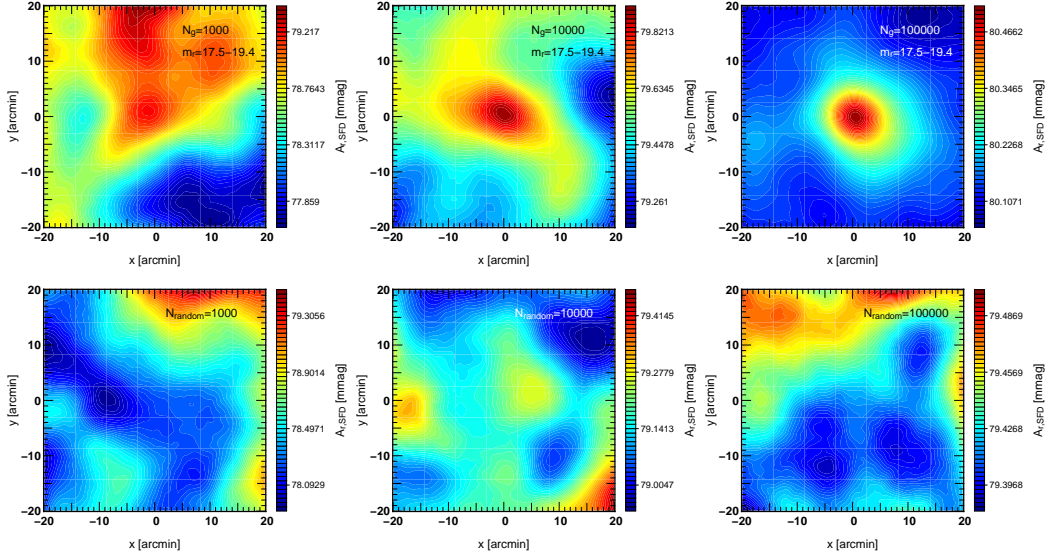


Fig. 4. Stacked images of the SFD map for $40' \times 40'$ regions; *Upper panels* are centered at the positions of SDSS galaxies of $17.5 < m_r < 19.4$, and *lower panels* show the reference images centered at randomly selected positions. Left, middle and right panels correspond to images stacking $10^3, 10^4, 10^5$ images.

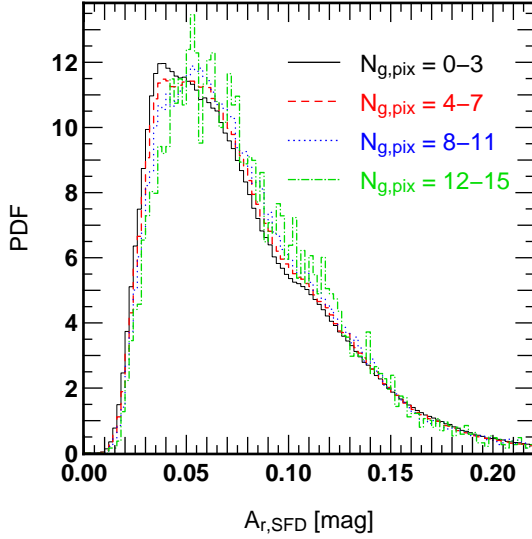


Fig. 3. The normalized probability density function (PDF) of $A_{r,SFD}$ corresponding to Figure 2.

location of galaxies according to their r -band magnitudes. The results are plotted in Figure 5. Thanks to the significantly large number of the SDSS galaxies, those images are highly circular, assuring that the signals do not originate from the Galactic contamination. All the angular radii of the images are very similar to the expected smoothing length of the SFD map ($= 6.1$ FWHM), and one may naively interpret that the central signal is dominated by the single galaxy contribution. As we will show below, however, this is not the case; in most cases the signal is rather dominated by the contribution from the nearby galaxies. Qualitatively this is understood from Figure 3 that shows the systematic increase of $A_{r,SFD}$ as

a function of numbers of galaxies in the pixel whose size is much smaller than the overall smoothing size of the SFD map.

To proceed more quantitatively, we attempt to model the radial profile of the stacked images as follows. Denote the angular profile of a single galaxy with r -band magnitude m_r as $\Sigma_g^s(\theta; m_r)$. Then the statistically averaged profile of the stacked images centered at the galaxy is given by

$$\Sigma_g^{\text{tot}}(\theta; m_r) = \Sigma_g^s(\theta; m_r) + \Sigma_g^c(\theta; m_r) + C, \quad (1)$$

where $\Sigma_g^c(\theta; m_r)$ denotes the clustering term corresponding to the contribution from the nearby galaxies, and C represents the background level of the extinction. Naively, C is expected to be independent of m_r and computed from the PDF of the extinction $P(A)$ (see Figure 3) as

$$C = \langle A \rangle \pm \frac{\sigma_A}{\sqrt{N_g}}, \quad (2)$$

where N_g is the number of stacked galaxy images, and the mean and rms are given by

$$\langle A \rangle = \int_0^\infty AP(A)dA, \quad (3)$$

$$\sigma_A^2 = \int_0^\infty A^2P(A)dA - \langle A \rangle^2. \quad (4)$$

As we see below, however, this is not the case. Therefore we treat C as a free parameter for each magnitude bin in the fitting analysis described below. Figure 6 plots $\langle A \rangle$ with quoted error-bars of σ_A as a function of $N_{g,\text{pix}}$.

The clustering term is written as

$$\Sigma_g^c(\theta; m_r) = \iint dm' d\varphi \Sigma_g^s(\theta - \varphi; m') \times w_g(\varphi; m', m_r) \frac{dN_g(m')}{dm'}, \quad (5)$$

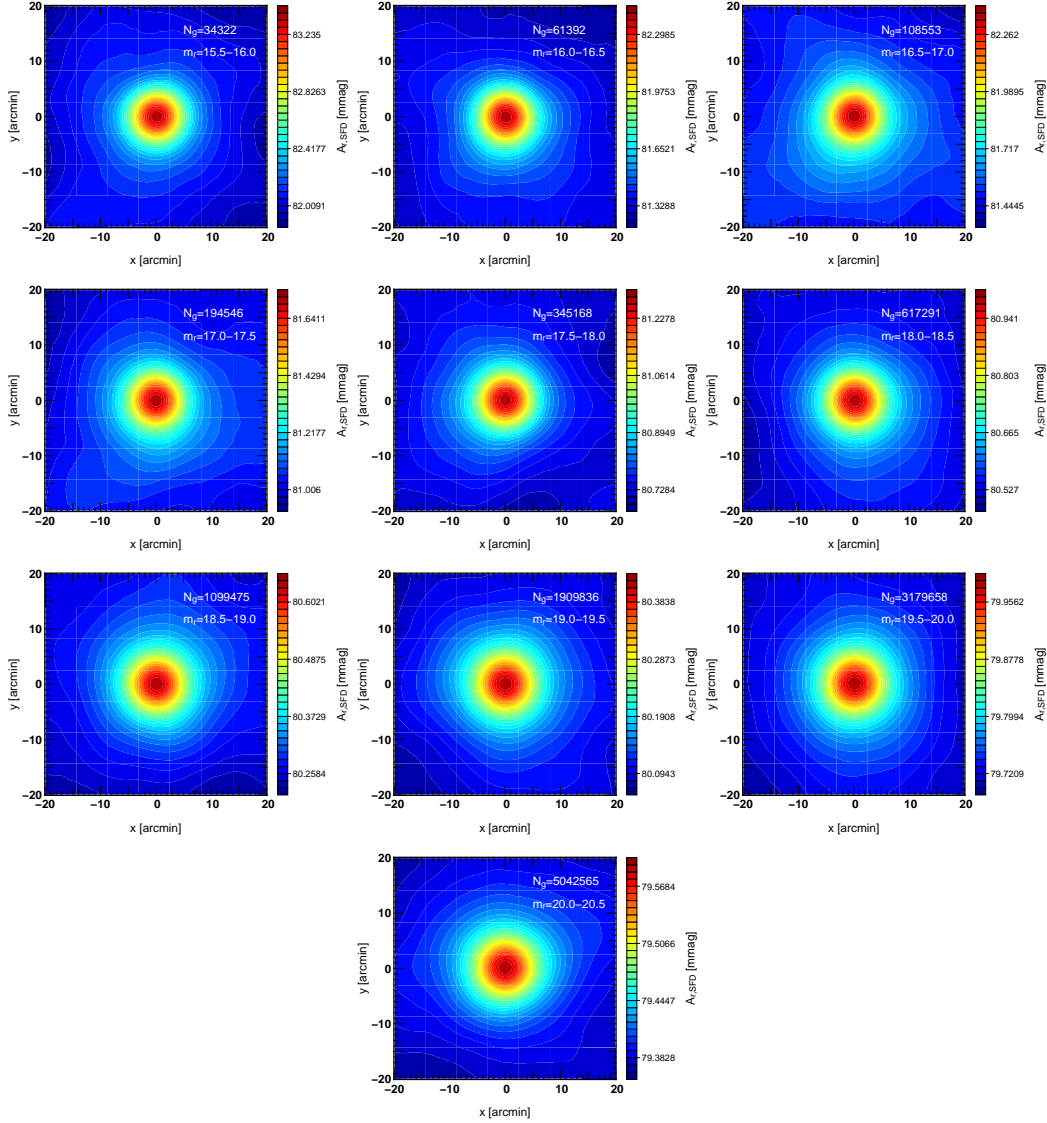


Fig. 5. Stacked images of the SFD map for $40' \times 40'$ centered at SDSS galaxies of different r -band magnitudes ($m_r = 15.5 \sim 20.5$ mag.) in 0.5 magnitude bin. The magnitude range and the number of galaxies in the range are denoted in each panel.

where $w_g(\varphi; m', m_r)$ is the angular galaxy cross-correlation function between magnitudes m' and m_r , and $dN_g(m')/dm'$ is the differential galaxy number density.

Given the large smoothing length of the SFD map (6.1 FWHM), a single galaxy profile is expected to be approximated by the circular Point Spread Function (PSF), independently of its intrinsic profile. Thus we adopt the Gaussian PSF profile:

$$\Sigma_g^s(\theta; m_r) = \Sigma_g^{s0}(m_r) \exp\left(-\frac{\theta^2}{2\sigma^2}\right), \quad (6)$$

where σ is the Gaussian width of the PSF. The Gaussian approximation of the PSF is justified in Appendix. Also we assume that the angular cross-correlation function is given as

$$w_g(\varphi; m', m_r) = K(m', m_r)(\varphi/\varphi_0)^{-\gamma}, \quad (7)$$

where the constants φ_0 and γ are assumed to be inde-

pendent of m' and m_r . We adopt $\gamma = 0.75$ (Connolly et al. 2002; Scranton et al. 2002), which is valid for $\varphi < 1^\circ$. With equations (6) and (7), equation (5) reduces to

$$\begin{aligned} \Sigma_g^c(\theta; m_r) &= \Sigma_g^{c0}(m_r) \exp\left(-\frac{\theta^2}{2\sigma^2}\right) \\ &\times {}_1F_1\left(1 - \frac{\gamma}{2}; 1; \frac{\theta^2}{2\sigma^2}\right), \end{aligned} \quad (8)$$

where ${}_1F_1(\alpha; \beta; x)$ is the confluent hypergeometric function, and

$$\begin{aligned} \Sigma_g^{c0}(m_r) &= 2\pi\sigma^2 \left(\frac{\varphi_0}{\sqrt{2}\sigma}\right)^\gamma \Gamma\left(1 - \frac{\gamma}{2}\right) \\ &\times \int dm' \Sigma_g^{s0}(m') K(m', m_r) \frac{dN_g(m')}{dm'}. \end{aligned} \quad (9)$$

Equation (8) results in the extended tail due to the clustering term in addition to the Gaussian tail of the single

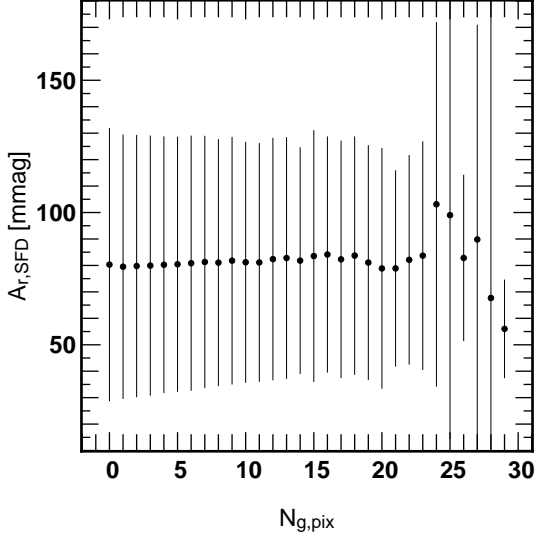


Fig. 6. Mean values of $A_{r,SFD}$ of pixels containing $N_{g,pix}$ plotted against $N_{g,pix}$. The quoted error bars indicate the corresponding rms.

central galaxy. The latter is negligible at $\theta \gg \sigma$, and the observed tail of the profile around galaxies is basically dominated by the clustering term.

The average radial profiles of the stacked images centered at photometric galaxies are plotted in Figure 7. Filled circles and triangles correspond to galaxies in the different r -band magnitude ranges in Figure 5, and the quoted error-bars represent rms in each circular bin of $\Delta\theta = 0''.33$. The solid curves are the best-fit model of equations (1), (6), and (8). In fitting those curves, we treat Σ_g^{s0} , Σ_g^{c0} , and C for each magnitude bin, and the width of PSF, σ as free fitting parameters. Here we assume that σ is independent of m_r , and fit it simultaneously for all profiles with different magnitudes. The resulting best-fit value of $\sigma = 3''.1$ is reasonable, given the resolution of the SFD map ($2''.59$ in Gaussian width) and the additional smoothing due to the $2''.37$ pixelisation and our cloud-in-cell interpolation.

The best-fit parameters for $\Sigma_g^{s0}(m_r)$ and $\Sigma_g^{c0}(m_r)$ are plotted in Figure 8. Even at the central position of the stacked images, the FIR signals are indeed dominated by the clustering term Σ_g^c rather than the single galaxy term (see Figure 9). Since the value of γ is somewhat uncertain and also depends on magnitudes, m_r and m'_r , we performed the same fitting analysis by varying the value for $0.65 < \gamma < 0.85$, which roughly covers the range of γ for our sample magnitudes. The dashed lines in Figure 8 show best-fit values for $\gamma = 0.65$, and dotted lines for $\gamma = 0.85$. Although the best-fit values of $\Sigma_g^{s0}(m_r)$ are affected by the choice of γ , especially for the faint magnitudes, the results for $\Sigma_g^{c0}(m_r)$ hardly change and still dominate the single term.

In reality, we did not anticipate this before performing the radial fits. Therefore we directly measure the angular cross-correlation of SDSS galaxies for comparison, and independently estimate the clustering term using equation

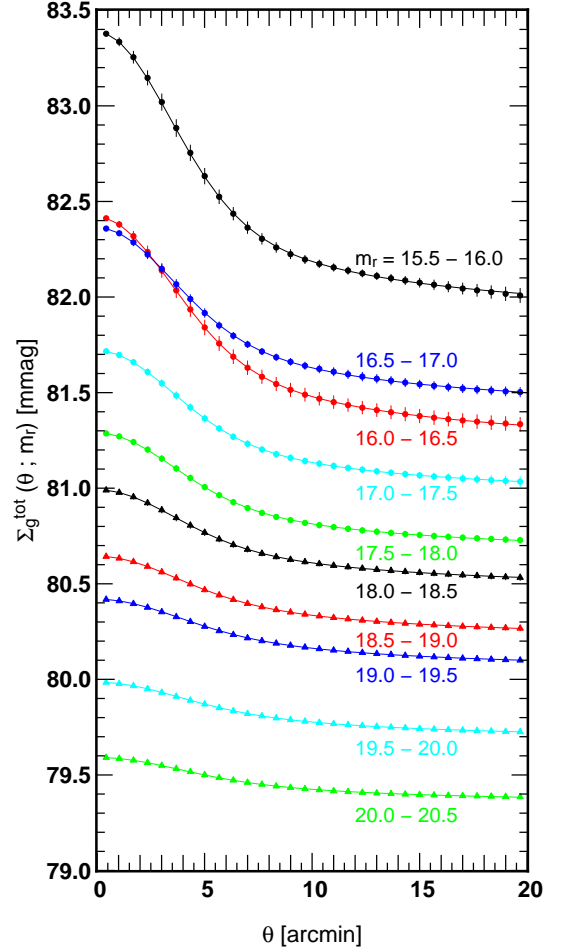


Fig. 7. Radial profiles of stacked galaxy images corresponding to Figure 5. Solid curves indicate the best-fit model of equation (1), (6), and (8).

(5), which we call $\Sigma_g^{c0}(\text{model})$. Dashed and Solid curves in Figure 10 indicate $\Sigma_g^{c0}(\text{model})$ and $\Sigma_g^{s0}(\text{fit}) + \Sigma_g^{c0}(\text{model})$, respectively. We still adopt $\Sigma_g^{s0}(\text{fit})$ (blue crosses), obtained by the profile-fits above, for the single term. The results indicate that resolved SDSS galaxies explain only 25~40% of the clustering term. This implies that the relation between r -band and FIR luminosity has significant scatter and/or substantial fraction of FIR sources are not resolved by the SDSS optical selection criteria. The estimated clustering term exceeds the single term by more than a factor of a few for faint magnitudes.

The fitted values of the background noise term C are plotted against m_r in Figure 11. According to our model, they should not depend on m_r , but it is not the case at all. A systematic decrease of C against m_r is clearly seen. We are not yet able to understand this systematic behavior. We repeated the same analysis by selecting those galaxies located in the inner contiguous regions ($160^\circ < \alpha < 220^\circ$, $5^\circ < \delta < 80^\circ$; see Figure 1). The results are plotted in red crosses after shifting 25 mmag, just for the ease of visual comparison. The fact that the value of C is also sensitive to the region of the map and the weaker m_r -dependence

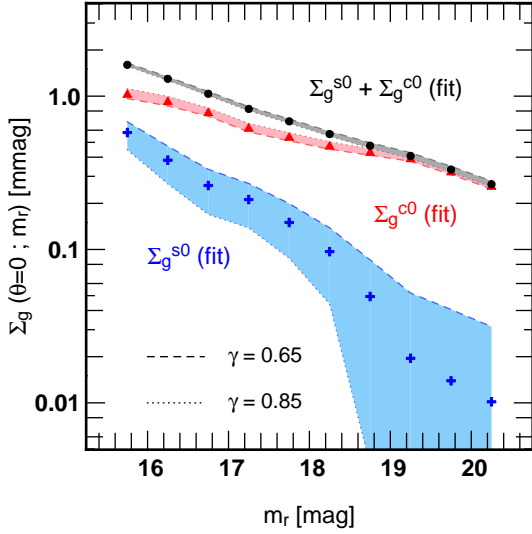


Fig. 8. Best-fit parameters characterizing the FIR emission of galaxies against their r -band magnitude. Crosses, triangles, and circles indicate the best-fit value of Σ_g^{s0} (fit), Σ_g^{c0} (fit), and Σ_g^{s0} (fit) + Σ_g^{c0} (fit), respectively, assuming $\gamma = 0.75$. Shaded regions indicate the variance of the best-fit parameters for $0.65 < \gamma < 0.85$. Dashed curve indicates the results for $\gamma = 0.65$ and dotted curve is for $\gamma = 0.85$.

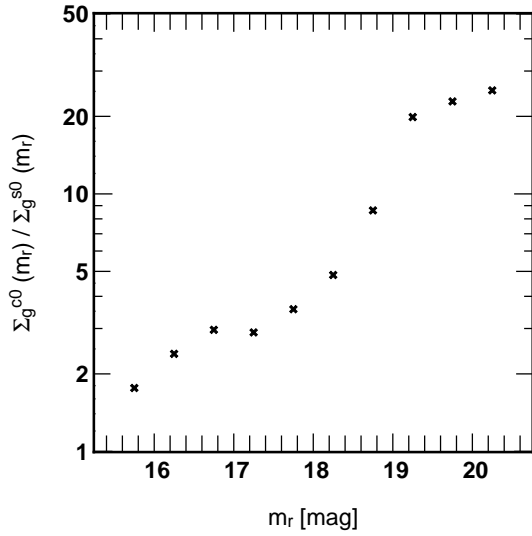


Fig. 9. Ratio of the clustering term and the central galaxy contribution as a function of the r -band magnitude of the central galaxy.

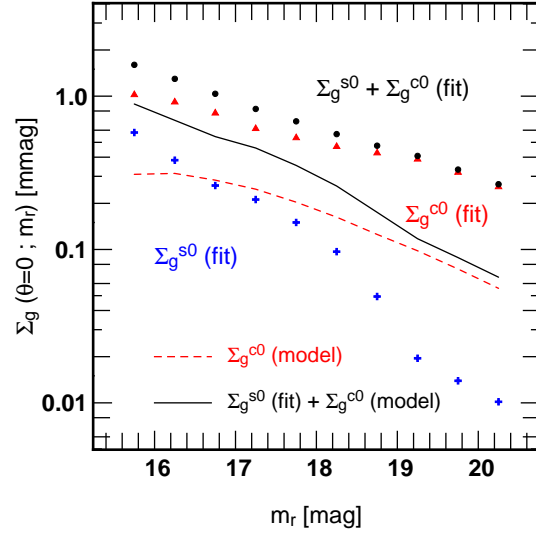


Fig. 10. The clustering term Σ_g^{c0} (model) estimated from the SDSS angular cross-correlation is plotted as a function of the r -band magnitude of the central galaxy (dashed curve). Solid curve indicates the sum of the single and clustering term Σ_g^{s0} (fit) + Σ_g^{c0} (model). The symbols are the same as Figure 8, and plotted for comparison.

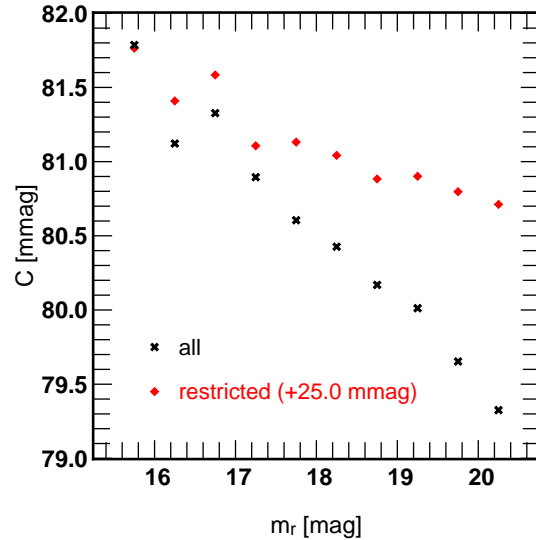


Fig. 11. The background noise level C against the r -band magnitude of the central galaxy. Black crosses indicate the results for all our sample and red ones are restricted in the inner regions shown as yellow lines in Figure 1.

in this case may imply that this is due to a subtle selection criterion difference of SDSS photometric galaxies as a function of the Galactic extinction itself, including the star-galaxy separation in different area, for instance. We do not investigate this issue in the present paper since our main finding is unlikely affected by the position dependent value of the background noise term. Actually, the best-fit values for other quantities are not sensitive to the particular choice of subregions in the SFD map.

Incidentally the small value of C with respect to the

general trend at $16.0 < m_r < 16.5$ is the reason why the corresponding profile in Figure 7 does not follow the systematic trend of the other profiles.

We note that, if σ is treated as a free parameter separately for different magnitudes, $\sigma(m_r)$, the resulting fits in the cases of $m_r > 19.0$ return a small negative value for Σ_g^{s0} . We found that this is simply due to the fact the total signal is dominated by the clustering term; the unambiguous extraction of the single galaxy contribution in those cases is difficult if we add another degree of freedom

in σ for each magnitude bin. In the case of $m_r < 19$, the best-fit values of σ are indeed almost independent of m_r and $\sigma \sim 3'.1$ as expected from our model assumption. This is why we constrained σ to be independent of m_r in the actual fitting procedure. This assumption does not affect the best-fit parameters except for Σ_g^{s0} with $m_r > 19$.

3. Implications

The fitting results presented in the previous section are model-independent in a sense that it does not assume any *a priori* relation between the r -band magnitude and the FIR emission of galaxies. Therefore the empirical correction of the SFD extinction for galaxies can be made from Figure 8. We note here that the correction is not limited to SDSS galaxies at all, and can be directly applied to future galaxy surveys as long as the r -band magnitude of galaxies is measured. This is because the dominant clustering term is contributed by galaxies that are not even resolved or identified in the SDSS galaxy catalog.

Nevertheless it is interesting to consider the underlying connection between the FIR emission and r -band magnitude of galaxies on the basis of the present result. Consider a galaxy with intensity profile $I_{100\mu\text{m}}(\theta)$ [MJy/sr]. Then its contribution to the r -band extinction should be

$$\Sigma_g^s(\theta; m_r) = \left[\frac{A_r}{E(B-V)} \right] \times p \times I_{100\mu\text{m}}(\theta), \quad (10)$$

where $A_r/E(B-V)$ and p are the conversion factors from the color excess $E(B-V)$ to the r -band extinction and from $100\mu\text{m}$ intensity to $E(B-V)$, and are given as 2.751 and 0.0184, respectively (Schlegel, Finkbeiner & Davis 1998). Integrating equation (10) over θ assuming the Gaussian profile, we obtain

$$2\pi\sigma^2\Sigma_g^{s0}(m_r) = \left[\frac{A_r}{E(B-V)} \right] \times p \times f_{100\mu\text{m}} \text{ [MJy]}. \quad (11)$$

Finally the $100\mu\text{m}$ flux, $f_{100\mu\text{m}}$ is translated to the $100\mu\text{m}$ magnitude:

$$m_{100\mu\text{m}} = -2.5 \log(f_{100\mu\text{m}}/3.63 \times 10^{-3} \text{ [MJy]}), \quad (12)$$

and equation (11) is rewritten in terms of m_r as

$$\Sigma_g^{s0}(m_r) = 36.0 \times 10^{-0.4m_{100\mu\text{m}}} \left(\frac{3'.1}{\sigma} \right)^2. \quad (13)$$

Since those magnitudes, m_r and $m_{100\mu\text{m}}$, should correspond to the same galaxy, their difference is equivalent to the ratio of their absolute luminosities, $L_{100\mu\text{m}}/L_r$. Thus estimated ratios are plotted in Figure 12. The fact that the ratio for a single galaxy is approximately constant indicates that the statistically averaged ratio of FIR and optical luminosities of galaxies are independent of the r -band magnitude, which is very reasonable. For comparison, we plot the ratio for adding the clustering term in FIR. In this case the integration of $\Sigma_g^s(\theta; m_r)$ over θ does not converge because our assumed value of $\gamma (= 0.75)$ is valid only for angular separation less than 1° . Thus we evaluate the flux simply by multiplying $2\pi\sigma^2$ as in the

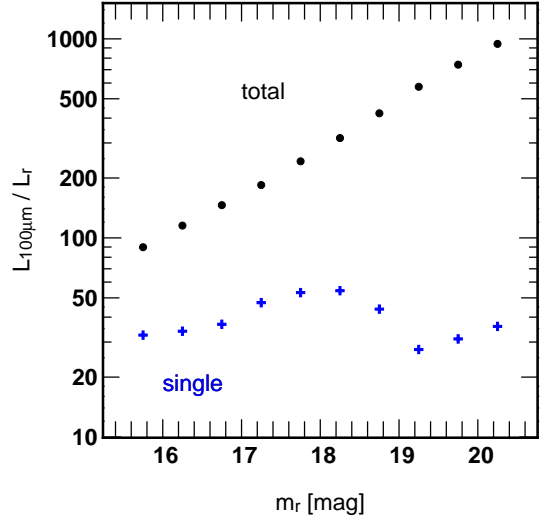


Fig. 12. Ratio of FIR and r -band luminosities as a function of the r -band magnitude of the central galaxy. Crosses indicate the ratio for single galaxy term, while circles include the clustering term as well.

case of the Gaussian profile. Therefore $L_{100\mu\text{m}}$ includes the contribution of other galaxies, but the total amplitude is subject to change depending on the more accurate profile at larger angular scales. The total ratio follows a clear single power-law and we believe that the wiggles of the ratio for single galaxies is not real but comes from the difficulty in separate the single galaxy contribution from the total signal as mentioned at the end of the previous section.

The relation between FIR and optical luminosities of galaxies can be directly probed from the sample of 3304 galaxies overlapped in the SDSS and PSCz (Saunders et al. 2000). We select the brightest SDSS galaxy locating within 2 arcmin from each PSCz galaxy as its counterpart. This procedure enables us to find SDSS optical counterparts for $\sim 95\%$ of the PSCz galaxies that are located in the SDSS survey region. We apply the K-correction based on the “K-corrections calculator” service (Chilingarian, Melchior, & Zolotukhin 2010) for r -band, and extrapolate the FIR spectral energy densities using second-order polynomials determined from 25, 60 μm flux for 100 μm (Takeuchi, Yoshikawa & Ishii 2003). Figure 13 is a scatter plot of $L_{100\mu\text{m}}$ (PSCz) and L_r (SDSS) for the PSCz–SDSS overlapped sample of galaxies. Figure 13 indicates an approximate linear relation between $L_{100\mu\text{m}}$ and L_r albeit with considerable scatters. The solid lines correspond to $L_{100\mu\text{m}}/L_r = 20$ and 50 for reference. Thus the approximate linear relation implied from Figure 12 is largely consistent with Figure 13 since the IRAS galaxies may be preferentially biased toward the FIR brighter ones than average. In turn, this confirms that our interpretation that Σ_g^s represents the contribution of a single galaxy.

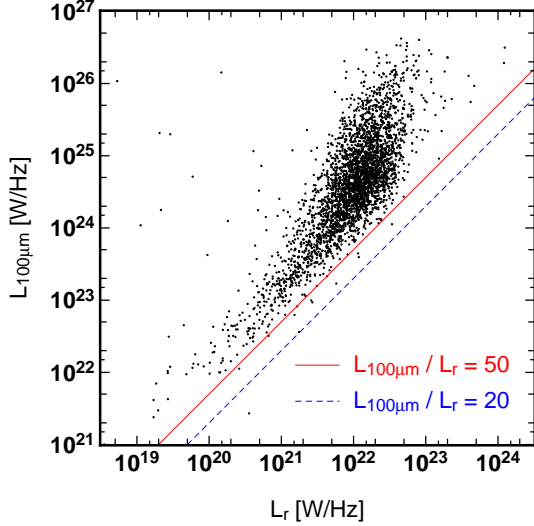


Fig. 13. Relation between $L_{100\mu\text{m}}$ and L_r for the IRAS/SDSS overlapped galaxies. The solid and dashed lines indicate $L_{100\mu\text{m}}/L_r = 20$, and 50, respectively.

4. Stacking analysis of SDSS DR6 quasars

Y07 did not find any definite anomaly between the quasar surface densities and A_{SFD} beyond the statistical errors. Nevertheless it is interesting to repeat the stacking analysis to SDSS quasar sample as well. Indeed as we show below, we found that a weaker but similar pattern of the enhanced extinction around stacked quasar images.

For this purpose, we use the SDSS DR6 photometric quasar sample (Richards et al. 2009a; Richards et al. 2009b). The analysis method is basically identical to that performed in subsection 2.3 except that we have to use the larger magnitude bins ($\Delta m_r = 1.0$) due to the limited number of the quasars as well as the weaker signature of the effect. The stacked images are plotted in Figure 14. As in the case of galaxies, we fit the radial profile to equations (1), (6), and (8) assuming that σ is independent of m_r . We find the best-fit value of $\sigma = 3.13$, which is similar to that for galaxy radial profile. The radial profiles and the best-fit curves are plotted in Figure 15.

Unlike galaxies, the profiles are not completely circular, and also the best-fit parameters do not exhibit regular behavior as a function of m_r . Part of the behavior may be due to the contamination of non-quasars objects in the photometric quasar sample. Therefore it would be better to repeat the analysis for the spectroscopic quasar sample, which we plan to do in due course. Nevertheless the results indicate a clear signal around the center of all the stacked images. If we look at Figure 9 in Y07 carefully, a very weak anomaly may be recognized for photometric quasars as well. This would be consistent with our current finding of the FIR emission around those quasars in the SFD map.

It is interesting to ask if the detected FIR emission around quasars originated from (1) quasars themselves, (2) their host galaxies, (3) neighbor galaxies due to the

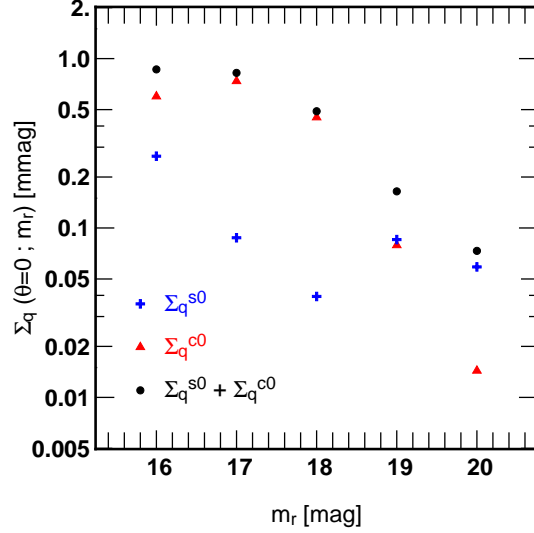


Fig. 16. Best-fit parameters characterizing the FIR emission of quasars against their r -band magnitude.

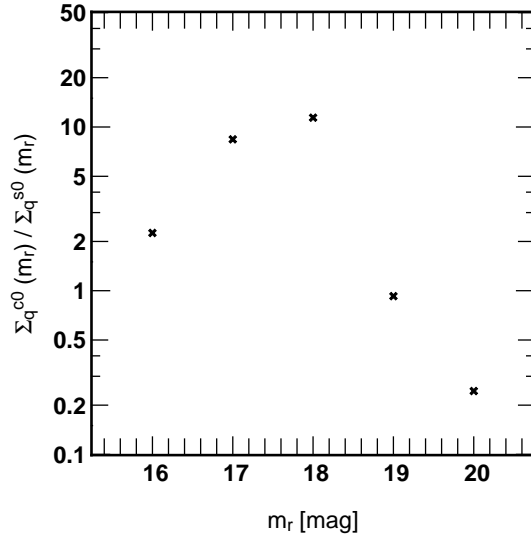


Fig. 17. Ratio of the clustering term and the central quasar contribution as a function of the r -band magnitude of the central quasar.

quasar-galaxy and/or quasar host galaxy-galaxy correlation, and/or (4) some other effects (lensing, for instance). Observational studies of quasar V-band luminosity M_q and that of the host galaxy M_g imply a very weak correlation, at most, with significant scatters. Typically a quasar is one or two magnitudes brighter than its host galaxy (Hamilton, Casertano, & Turnshek 2008; Letawe, Letawe, & Magain 2010). Given those combined with the results for galaxies discussed in §3, the signal may be ascribed to the possibility (3). This deserves further investigation, and we are currently working on the analysis using the WISE (Wright et al. 2010) and IRAS (Wheelock et al. 1994) data to explore the quasar-galaxy correlation in FIR.

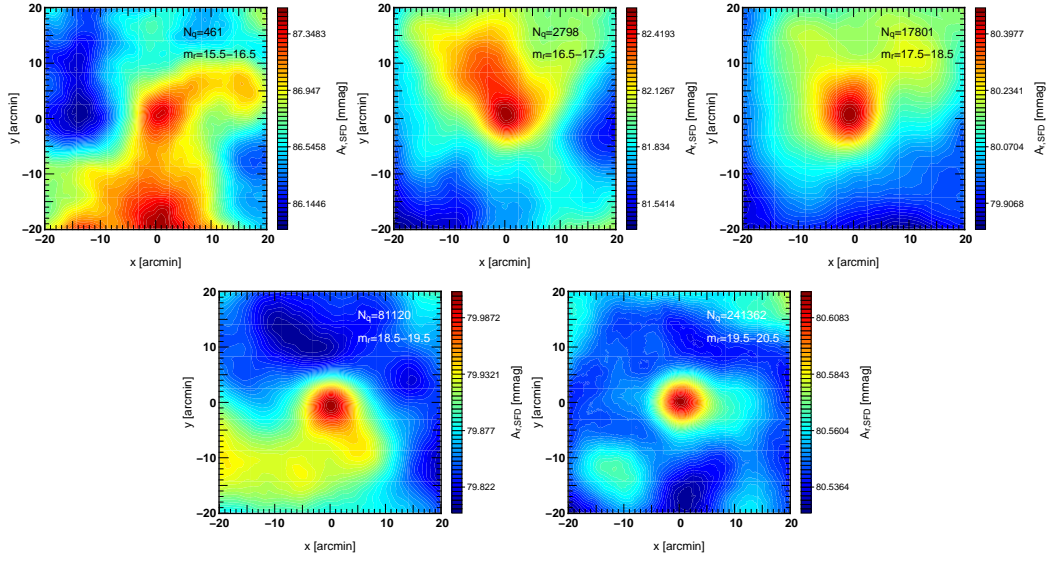


Fig. 14. Stacked images of the SFD map for $40' \times 40'$ centered at SDSS quasars of different r -band magnitudes ($m_r = 15.5 \sim 20.5$ mag) in 1.0 magnitude bin. The magnitude range and the number of quasars in the range are denoted in each panel.

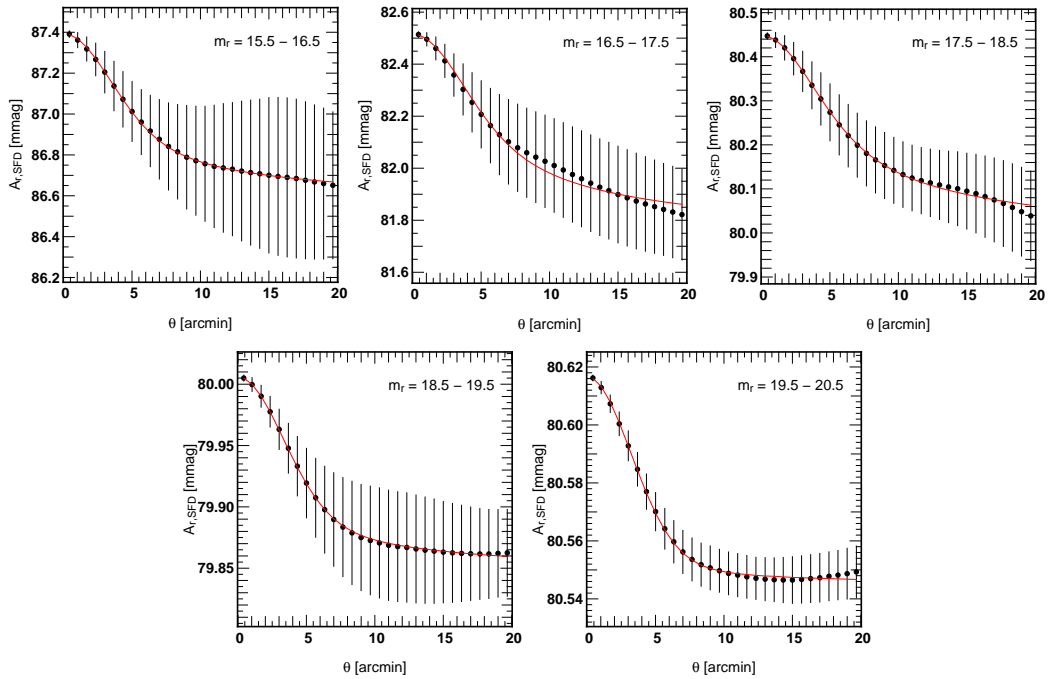


Fig. 15. Radial profiles of stacked quasar images corresponding to Fig. 14. Solid curves indicate the best-fit model of equation (1), (6), and (8).

5. Conclusions

We have detected the small but systematic contamination in the SFD Galactic extinction map due to FIR emission from galaxies. The amount of the contamination of the order of mmag is very small and may be negligible for most astronomical purposes. Nevertheless, the contamination is intrinsically correlated with the large-scale structure of the universe traced by galaxies, and therefore should be kept in mind in precision cosmological measure-

ments. Indeed even such a small contamination leads to a relatively large anomaly of the galaxy surface number density as a function of A_{SFD} discovered by Yahata et al. (2007).

Our major result is that a galaxy of r -band magnitude m_r has an additional *contribution* to the SFD Galactic extinction by an amount of

$$\Delta A_r(m_r) = 0.087 \times 10^{0.41(18-m_r)} \text{ [mmag]}, \quad (14)$$

due to the FIR emission from itself (single term), and

$$\Delta A_r(m_r) = 0.64 \times 10^{0.17(18-m_r)} \text{ [mmag]}, \quad (15)$$

including the contribution from nearby galaxies (clustering term: Figure 18). Note that since the SFD determination of conversion factor p has statistical and systematic uncertainties of approximately 8%, equation (14) and (15) would have the similar level of uncertainties.

One possible method to correct the SFD map is to subtract all the contributions of identified galaxies; the corrected extinction at position θ is obtained as

$$A'_r(\theta) = A_{r,\text{SFD}}(\theta) - \sum_j \Sigma_g^s(\theta_j - \theta; m_r^j), \quad (16)$$

where θ_j is the position of the j -th galaxy with its r -band magnitude of m_r^j . Note that this correction ignores contributions of other than the identified galaxies; if the SDSS DR7 photometric galaxy catalog is used, only contributions from those galaxies listed in the catalog are corrected. We could use $\Sigma_g^{\text{tot}}(\theta_j - \theta; m_r^j)$ in equation (16), including the clustering term Σ_g^c . In that case, however, it would over-count the true contribution especially when the pixel has many nearby galaxies. In turn it is interesting to examine the extent of which the anomaly detected by Y07 is explained by the SDSS DR7 galaxies alone, by applying the correction on the basis of equation (16).

Most likely improved correction formulae than equation (14) and (15) may be obtained by further dividing galaxy samples according to their colors, fully exploiting the multi-band photometries of SDSS DR7. Also similar stacking analyses of various current/future sky maps in different wavelengths, e.g., WISE, IRAS, AKARI (Murakami et al. 2007), WMAP (Bennett et al. 2003), Planck (Tauber et al. 2010) among others, are interesting to make sure of their validity and/or put constraints on the possible contamination.

We would like to emphasize also that the present methodology is useful to derive statistical relations among galaxy parameters in different bands and to infer the angular cross-correlation of galaxies, much beyond the magnitude limit for individual galaxy surveys. The results for those directions will be presented elsewhere.

We thank Issha Kayo, Shirley Ho, Teruyuki Hirano, Atsushi Taruya, Toru Yamada, Brice Ménard, Takashi Onaka, Hideyuki Izumiura, and Takao Nakagawa for useful discussions. We also thank an anonymous referee for many valuable comments. This work is supported in part from the Grant-in-Aid No. 20340041 by the Japan Society for the Promotion of Science. Y.S. and T.K. gratefully acknowledge supports from the Global Scholars Program of Princeton University and from Global Center for Excellence for Physical Science Frontier at the University of Tokyo, respectively.

Funding for the SDSS and SDSS-II has been provided by the Alfred P. Sloan Foundation, the Participating Institutions, the National Science Foundation, the U.S. Department of Energy, the National Aeronautics and Space Administration, the Japanese Monbukagakusho, the Max Planck Society, and the Higher Education

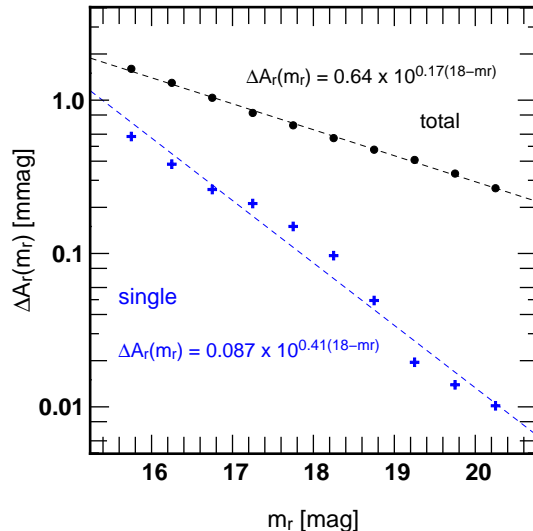


Fig. 18. ΔA_r as a function of r -band magnitude of the central galaxy. Crosses indicate the single galaxy term, while circles include the clustering term as well.

Funding Council for England. The SDSS Web Site is <http://www.sdss.org/>.

The SDSS and SDSS-II are managed by the Astrophysical Research Consortium for the Participating Institutions. The Participating Institutions are the American Museum of Natural History, Astrophysical Institute Potsdam, University of Basel, Cambridge University, Case Western Reserve University, University of Chicago, Drexel University, Fermilab, the Institute for Advanced Study, the Japan Participation Group, Johns Hopkins University, the Joint Institute for Nuclear Astrophysics, the Kavli Institute for Particle Astrophysics and Cosmology, the Korean Scientist Group, the Chinese Academy of Sciences (LAMOST), Los Alamos National Laboratory, the Max-Planck-Institute for Astronomy (MPIA), the Max-Planck-Institute for Astrophysics (MPA), New Mexico State University, Ohio State University, University of Pittsburgh, University of Portsmouth, Princeton University, the United States Naval Observatory, and the University of Washington.

Appendix. IRAS Point Spread Function

In subsection 2.3, we decompose the stacked radial profiles into single and clustering terms, assuming the Gaussian PSF. Since the IRAS PSF is known to be very complex, we need to check the validity of this assumption. For the purpose of determining the PSF directly, we perform similar stacking analysis with SDSS stars.

More specifically, we select spectroscopic stars brighter than $m_r = 17.0$ (12823 stars in total) from the SDSS DR7 catalog. We first stack the SFD map centered on those SDSS stars as we did for SDSS galaxies and quasars, but we find no significant signature. This is mainly because the bright point sources in the IRAS catalogue are already removed from the SFD map. Therefore we go back

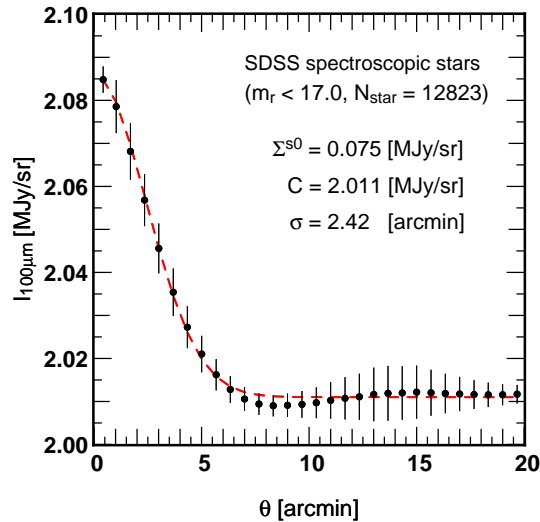


Fig. 19. Radial profiles of stacked star images. The dashed curve indicates the best-fit Gaussian profile.

to the original ISSA $100\mu m$ diffuse map, and perform the stacking analysis. The resulting stacked average radial profile of the SDSS stars is shown in Figure 19. The data points are well approximated by a single Gaussian. The best-fit Gaussian shown in the dashed curve has a width of $\sigma = 2''.42$, which is slightly smaller than that found in subsection 2.3. This is understood because since the SFD map is constructed by further smoothing the original ISSA map. Thus we conclude that our assumption of the Gaussian PSF is valid.

References

- Bennett, C. L., et al. 2003, *ApJ*, 583, 1
 Chilingarian, I. V., Melchior, A.-L., & Zolotukhin, I. Y. 2010, *MNRAS*, 405, 1409.
 Connolly, A. J., et al. 2002, *ApJ*, 579, 42
 Fukugita, M., Ichikawa, T., Gunn, J. E., Doi, M., Shimasaku, K. & Schneider, D. P. 1996, *AJ*, 111, 1748
 Gunn, J. E., et al. 1998, *AJ*, 116, 3040
 Gunn, J. E., et al. 2006, *AJ*, 131, 2332
 Hamilton, T.S., Casertano, S., & Turnshek, D.A. 2010, *ApJ*, 678, 22
 Hogg, D. W., Finkbeiner, D. P., Schlegel, D. J. & Gunn, J. E. 2001, *AJ*, 122, 2129
 Ivezić, Ž., et al. 2004, *Astronomische Nachrichten*, 325, 583
 Letawe, Y., Letawe, G., & Magain, P. 2010, *MNRAS*, 403, 2088
 Murakami, H., et al. 2007, *PASJ*, 59, 369
 Padmanabhan, N., et al. 2008, *ApJ*, 674, 1217
 Pier, J. R., Munn, J. A., Hindsley, R. B., Hennessy, G. S., Kent, S. M., Lupton, R. H., & Ivezić, Ž. 2003, *AJ*, 125, 1559
 Richards, G. T., et al. 2009a, *AJ*, 137, 3884
 Richards, G. T., et al. 2009b, *ApJS*, 180, 67
 Saunders, W., et al. 2000, *MNRAS*, 317, 55
 Schlegel, D., Finkbeiner, D., & Davis, M. 1998 *AJ*, 500, 525
 Scranton, R., et al. 2002, *ApJ*, 579, 48.
 Smith, J. A., et al. 2002, *AJ*, 123, 2121
 Stoughton, C., et al. 2002, *AJ*, 123, 485

- Takeuchi, T. T., Yoshikawa, K. & Ishii, T. T. 2003, *ApJL*, 587, L89
 Tauber, J. A., et al. 2010, *A&A*, 520, A1
 Tucker, D. L., et al. 2006, *Astronomische Nachrichten*, 327 821
 Wheelock, S. L. et al. 1994, *IRAS Sky Survey Atlas: Explanatory Supplement*, JPL Publication 94-11 (Pasadena: JPL)
 Wright, E. L., et al. 2010, *AJ*, 140, 1868
 Yahata, K., Yonehara, A., Suto, Y., Turner, E.L., Broadhurst, T., & Finkbeiner, D. 2007, *PASJ*, 59, 205 (Y07)
 York, D. G., et al. 2000, *AJ*, 120, 1579